Heavy Flavour Production at HERA

Christoph Grab
On behalf of the H1 and ZEUS Collaborations
Institute for Particle Physics, ETH-Zürich, CH-8093 Zürich, Switzerland

Measurements of charm production in lepton-proton collisions at a centre-of-mass energy of $\sqrt{s} = 300$ GeV performed at HERA by the experiments H1 and ZEUS are reviewed. Final states containing charm are mainly identified by reconstruction of $D^{*\pm}$ and J/Ψ mesons. The results cover the region in 4-momentum transfer squared Q^2, from photoproduction ($Q^2 \approx 0$) to deep-inelastic scattering at high Q^2. The experimental results are compared with theoretical predictions, based primarily on QCD and in some cases on phenomenological models inspired by Regge-theory.

1 Introduction

The study of heavy quark production in lepton-proton scattering provides an important testing ground for the standard model. At the electron-proton collider HERA with an $e-p$ centre-of-mass energy $\sqrt{s} = 300$ GeV, heavy quarks are produced predominantly by the *photon gluon fusion* process $\gamma g \rightarrow c\bar{c}$, where a real or virtual photon emitted by the electron [a] and a gluon from the proton generate a $c\bar{c}$ pair. In this case colour is transferred from the proton so that the proton breaks up (inelastic scattering). In general, also elastic scattering may occur where no colour is transferred and the proton can remain intact (diffractive interactions).

The dominant contribution to charm production is due to exchange of an almost real photon *(photoproduction)*, where the negative squared four-momentum transfer carried by the photon is $Q^2 \approx 0$. The charm quarks hadronize and are then either detected as "open charm", *i.e.* in final states with charmed hadrons, or alternatively as "hidden charm" states, such as J/Ψ .

The kinematics of charm production is described by three independent variables, the centre-of-mass energy $\sqrt{s}$, the photon four-momentum squared $q^2 = -Q^2$ and either one of the scaling variables $y = (q \cdot P / l \cdot P)$, the inelasticity of the ep-interaction, or Bjorken-x $x = Q^2/(2P \cdot l)$. Here P and l denote the four-momentum of the proton and the electron, respectively. The $\gamma - p$ centre-of-mass energy squared is given by $W^2_{\gamma p} = W^2 \approx y \cdot s - Q^2$.

The results presented here are based upon about 10 pb^{-1} of data recorded by the H1 [1] and ZEUS [2] detectors during 1994 and 1995, when positrons and protons were collided head-on with energies of 27.5 GeV and 820 GeV.

[a] Hereafter, a reference to electron implies a reference to either electron or positron.

2 Open Charm Production

The description of inelastic open charm production is based on perturbative QCD (pQCD). In leading order (LO) the direct process of photon-gluon fusion (BGF of $\mathcal{O}(\alpha\alpha_s)$, i.e. $\gamma g \to c\bar{c}$) is the dominant contribution. In photoproduction, resolved photon interactions ($\sim \mathcal{O}(\alpha/\alpha_s) \times \mathcal{O}(\alpha_s^2)$ i.e. $gg \to c\bar{c}, q\bar{q} \to c\bar{c}$) contribute as well and lead to the notion of photon structure function. However, beyond LO *only the SUM* of direct and resolved processes is a well defined quantity.

The QCD calculations in NLO exist in several schemes: massive and massless ones. Both assume the scale to be hard enough (i.e. α_s small enough) to render pQCD feasible and the factorization theorem valid. The *massive approach* is a fixed order (in α_s) pQCD calculation (FOPT) with a massive charm quark ($m_c \neq 0$), and assumes the number of active flavours in the proton to be three ($N_f = 3$) plus the gluon. The charm quark is only produced at the perturbative level. The massive calculations are considered reliable in the low p_T-regime, in particular for σ_{tot}, and they agree pretty well with measurements done e.g. in $p\bar{p}$-experiments. However, this approach breaks down for large scales (see below) $p_T \gg m_c$ because no large-p_T resummation is done (the IS and FS collinear divergencies are $\sim ln(p_T^2/m_c^2)$).

In the *massless approach* the charm quark mass is assumed zero, and the number of active flavours is four. That is, charm is an active flavour in the proton and the photon, and hence additional processes may occur ($cg \to cg$, $cq \to cq$, ...). Within this approach the final state collinear divergencies are absorbed into the fragmentation functions. The large logarithms (high-p_T) are resummed by evolving the parton density functions (PDF) and fragmentation functions (FF) to the relevant scale. There are two different treatments of the fragmentation part, a coherence treatment [3] and the perturbative fragmentation function approach PFF [4], which have been shown to be equivalent [5]. The massless approach is indispensable for $p_T \gg m_c$, however it breaks down for $p_T \leq m_c$. Both massive and massless schemes have been successfully applied in photoproduction. In DIS the FOPT has been in use sofar [6,7].

In a third approach the features of these two methods are combined. The *variable flavour number scheme* (VFNS) [8] adjusts the number of active partons N_f according to the relevant scale. It applies the FOPT with a massive c-quark at low scales and treats the c-quark similar to massless quarks ($N_f = 4$) for scales much above the mass m_c. It is applicable for inclusive quantities such as σ_{tot}, F_2^c etc.

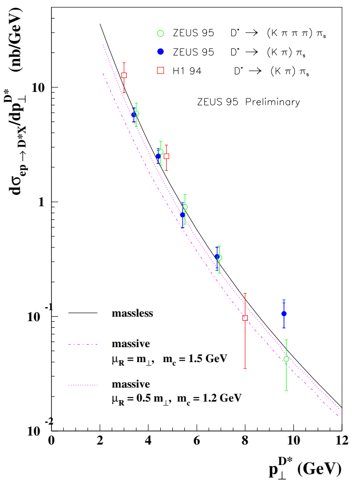

Figure 1: $d\sigma/dp_t$ distribution in photoproduction data for $Q^2 < 5(4)$ GeV^2 for ZEUS (H1). Overlaid are NLO QCD predictions in the massles (solid) and massive (dotted) scheme.

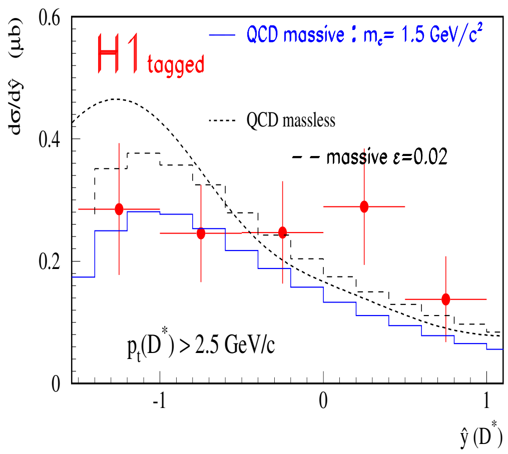

Figure 2: $d\sigma/d\hat{y}$ distribution tagged data. Comparison with NLO QCD massive calculations with $\epsilon_{Peterson} = 0.06$ (solid for $m_c = 1.5$) and $\epsilon_{Peterson} = 0.02$ (dashed). Top curve (dotted) shows NLO QCD massless prediction.

2.1 D-meson Photoproduction [9,10]

D^* mesons are identified in the H1 and ZEUS detectors by the decay $D^{*+} \to D^0\pi^+$, $D^0 \to K^-\pi^+$or $K^-\pi^+\pi^-\pi^+$, in the *visible* kinematic region where the transverse momentum of the D^* meson is greater than 2.5 GeV (3.0 GeV in the ZEUS analysis) and the laboratory rapidity $\hat{y}$ between -1.5 and 1.0. In the photoproduction analysis, events with $Q^2 > 4$ GeV^2 are rejected by insisting that the scattered electron is not found in the main part of the detector.

The visible differential distribution in $d\sigma/dp_t$ for untagged data ($Q^2 < 5(4)$ GeV^2 for ZEUS (H1)) is shown in fig.1. Overlaid are the predictions by the NLO QCD calculations [b]. Both massless (solid) and massive (dotted) approaches describe the shape well, the massive ones however is slightly below the data for the given choice of parameters (see below).

[b] The scales involved are the renormalization scale μ_r, the hadron and photon factorization scales μ_{Fh} and $\mu_{F\gamma}$, and are customarily given relative to the charm quark mass m_c. In the case of FOPT in photoproduction the values are: $\mu = m_T = \sqrt{m_c^2 + p_T^2}$; and $\mu_r = \mu; \mu_{Fh} = \mu_{F\gamma} = 2\mu$.

The differential distribution in $d\sigma/d\hat{y}$ for H1 tagged data ($Q^2 < 0.01$ GeV^2) is shown in fig.2. Overlaid are the predictions by the NLO QCD calculations. The massive calculation (solid line with PDFs MRSG and GRV-HO, $m_c = 1.5$ GeV), using a parameter $\epsilon_{Pete} = 0.06$ to describe fragmentation according to ref.[11], does not give a very good description of the data shape. Another choice for the parameter $\epsilon_{Pete} = 0.02$ increases the overall normalization and enhances the low $\hat{y}$-region (dashed). Thus it approaches closely the prediction of the massless calculation (dotted top line with PDFs CTEQ4M + GRV-HO) using a parameter $\epsilon_{Pete} = 0.0674$ as obtained from refitting the e^+e^--data by ref.[3]. A similar distribution has also been obtained recently by ref.[5], who in the massless framework of PFF refitted e^+e^--data (Argus and LEP) finding a best value $\epsilon_{Pete} = 0.02$. The question remains how much of the observed difference is due to fragmentation functions and how much originates from higher order corrections. This clearly indicates the necessity for a completely consistent treatment of both the cross-section calculation in the HERA frame and the extraction of the fragmentation parametrisation from other experiments.

However, an adjustment of ϵ_{Pete} alone does not result in a proper description of the data. There exists some discrepancy in the forward region, the clarification of which requires more data. The visible range is found to be fairly insensitive to the choice of PDF parametrizations, which are most distinctive unfortunately in the hard-accessible low-p_T region for the proton and in the large-$\hat{y}$ region for the photon.

The total photoproduction cross-section $\sigma(\gamma p \rightarrow c\bar{c}X)$ is calculated by extrapolating from the visible region to the total phase space, and by using the fragmentation fraction $B_{c\rightarrow D^*} = 0.260$ [12] and assuming a photon flux as given by the Weizsäcker-Williams Approximation [13]. The result is shown in figure 3 where the inner error bars represent the combined statistical and experimental systematic errors, and the outer error bars include the large uncertainty in the extrapolation due to the possible choices of parton density parametrizations. The prediction of a NLO QCD calculation [14] is shown for two extreme values of the renormalization scale as indicated, covering a factor of four in range. A strong rise of the photoproduction cross-section of charm with $W_{\gamma p}$ is observed, in good agreement with the QCD predictions.

2.2 D-meson Production in Deep-Inelastic Scattering [15,16]

The production of D^* and D^0 has been studied in events with an identified scattered electron with $10 < Q^2 < 100$ GeV^2.

Differential distributions $d\sigma$ are shown in fig. 4 in the variables $p_T(D^*)$, $\eta(D^*)$, $W_{\gamma^* p}$ and Q^2. A comparison with predictions based on massive pQCD

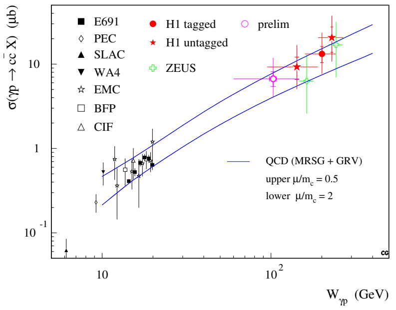

Figure 3: Total charm photoproduction cross-section as a function of $W_{\gamma p}$, including results from fixed-target experiments, and predictions of NLO QCD calculations [14] with MRSG and GRV-G HO parton density parametrizations. H1 'tagged' refers to events with the scattered e^+ detected in the low angle electron tagger.

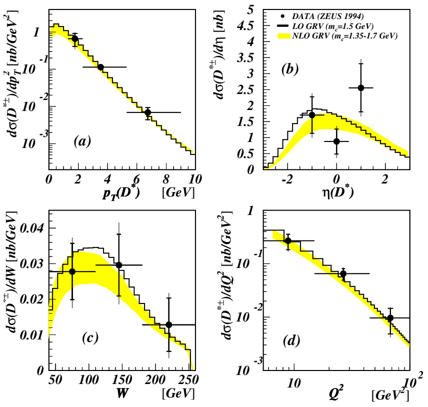

Figure 4: Differential cross-sections in DIS ($Q^2 > 5$ GeV^2). Zeus 1994 data (dots), pQCD LO (histogram) and NLO (band indicating $1.35 < m_c < 1.7$ GeV).

in NLO [6] reveils a fairly good agreement with the data for c-masses around 1.5 GeV. Extrapolating from the visible D cross-sections to the full $c\bar{c}$ cross-sections introduces less uncertainty than in the photoproduction case. The cross-sections are shown in figure 5 in the form of $F_2^{c\bar{c}}$, the charm contribution to the proton structure function, where

$$\frac{d^2\sigma^{c\bar{c}}}{dxdQ^2} = \frac{2\pi\alpha^2}{Q^4 x}\left[1+(1-y)^2\right] F_2^{c\bar{c}}\left(x, Q^2\right). \tag{1}$$

The results at HERA are consistent with each other, and extend the range of $F_2^{c\bar{c}}$ measurements by $\sim \mathcal{O}(100)$ towards smaller x-values with respect to lower energy data (EMC). Comparing the EMC with the HERA values exhibits a large increase of $F_2^{c\bar{c}}$ towards smaller x values, in good agreement with the NLO QCD interpretation of the HERA measurements on the proton structure function. The measured ratio $F_2^{c\bar{c}}/F_2$ is found to be compatible with being constant over the visible kinematic range, with an average value of about 0.25 seen by both the H1 and ZEUS experiments.

3 Charmonium Production

Studies of charmonium production allow to probe the strong interaction physics in the transition region between the perturbative QCD regime and non-pertur-

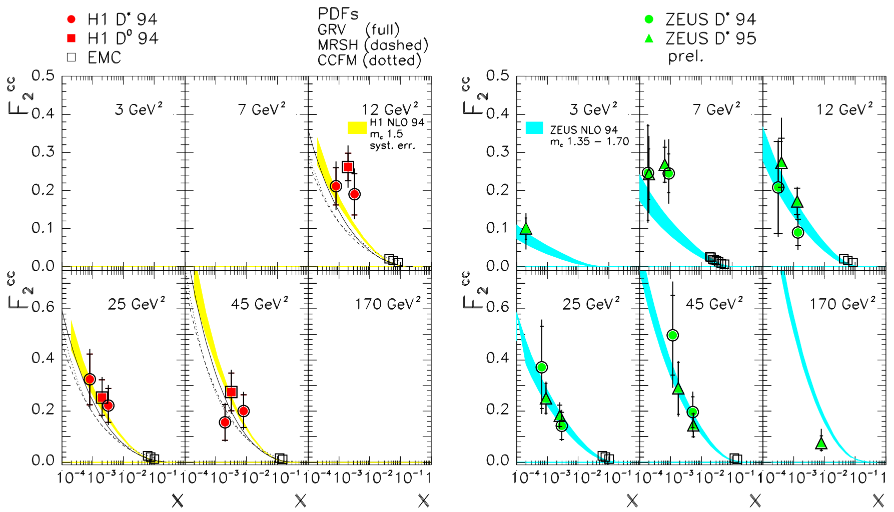

Figure 5: Charm contribution $F_2^{c\bar{c}}$ to the proton structure function, as measured by H1 (left) and ZEUS (right). The shaded bands represent predictions of the NLO QCD fits to the H1 and ZEUS F_2 measurements, respectively. At left are included also NLO predictions based on the gluon densities GRV-HO (solid), MRSH (dashed) and CCFM (dotted).

bative phenomenological models, where long range or soft interactions are considerable. The different production processes are here classified in terms of *elastic* and *inelastic* processes, depending on whether the proton stays intact or breaks up. On the experimental side, the separation is achieved by means of the *inelasticity* variable $z \equiv E_{J/\psi}/E_\gamma$ in the proton rest frame, with values of 1 for purely elastic, < 0.9 for inelastic and < 0.25 for resolved γp-interactions. J/ψ mesons are experimentally identified by their decays to lepton pairs.

3.1 Inelastic J/Ψ Production [17,18]

Predictions for the direct inelastic production of J/Ψ are based on the photon-gluon fusion mechanism, where the photon participates in the hard interaction with a gluon from the proton to form a $c\bar{c}$ pair. The hard interaction is calculable in perturbative QCD, and the production is sensitive to the gluon content of the proton. To achieve a colourless J/ψ state at least one further gluon must be involved in the interaction. In the colour-singlet model [19,20] the radiation of a gluon from a $c(\bar{c})$ line to form a colourless $c\bar{c}$ state is part of the hard interaction, whilst in the colour-octet model [24] the transition from the coloured

$c\bar{c}$ state produced in the hard sub-process proceeds non-perturbatively.

The cross-section measurements are restricted to the range in z between 0.45 and 0.9, where the contributions from resolved photon events and diffractive production are small. For comparison with NLO QCD calculations [20] in the colour-singlet model, cross-section determinations are restricted to the kinematic region $p_t(J/\psi) > 1$ GeV.

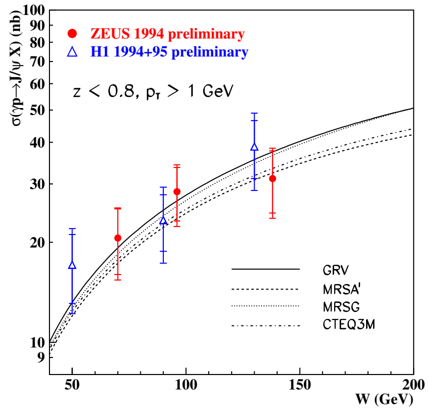

Figure 6: Inelastic photoproduction cross-sections for J/ψ, compared to NLO and LO QCD calculations in the colour-singlet model [20] based on the parton density parametrizations MRSG, GRV-LO and MRSA'.

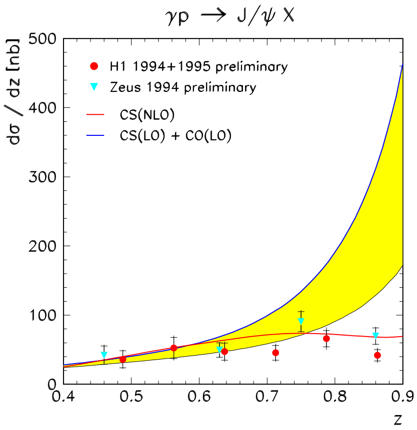

Figure 7: Inelastic differential photoproduction cross-section for J/Ψ , compared to predictions of the colour-singlet and colour-octet models [24] in LO (solid), and colour-singlet in NLO (dotted). The band represents the uncertainty in the CO+CS model calculation.

Figure 6 shows the direct inelastic photoproduction cross-section of J/ψ as a function of $W_{\gamma p}$ for $z < 0.8$, with predictions from NLO QCD calculations [20] based on various proton structure parametrizations. A strong rise in the cross-section with $W_{\gamma p}$ is observed which, within this model, is reflecting the rising gluon content of the proton towards low x. The results are not sensitive enough to distinguish between different parametrizations of the gluon content of the proton. The differential cross-section in z, depicted in fig. 7, is also well reproduced by calculations based on the colour-singlet model, but contains no indication of the sharp rise towards high z which is predicted in the colour-octet model if the normalization is chosen to fit the CDF data [21].

3.2 Elastic J/Ψ Production[17,22]

Elastic vector meson production at low scales is well described by an interaction mediated by a 'soft pomeron'[23], and the cross-section is predicted to be proportional to $W_{\gamma p}^{\delta}$ with $\delta = 0.32$. At larger scales, assuming that the charm quark mass offers a hard scale[25], the pomeron may be replaced by gluon ladders calculable in perturbative QCD. In this case the cross-section is proportional to the square of the gluon density of the proton at Bjorken $x \approx m_{J/\psi}^2/W_{\gamma p}^2$, and a much steeper rise with $W_{\gamma p}$ than in the soft pomeron case is expected. Cross-sections for the elastic interaction $\gamma p \to J/\psi p$ are measured in events where nothing but the decay products of the J/ψ meson are detected, and the remaining inelastic contamination is estimated. A strong rise of the cross-section with increasing $W_{\gamma p}$ is observed (figure 8), which is significantly beyond that expected for interactions mediated by a soft pomeron ($\delta = 0.32$). Rather, a value $\delta = 0.60$ provides a better fit to measurements.

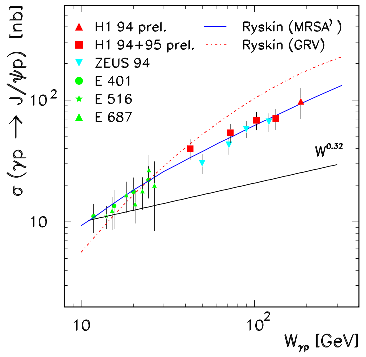

Figure 8: Elastic photoproduction cross-section for J/ψ vs $W_{\gamma p}$. Parametrizations of the $W_{\gamma p}$ dependence as $W_{\gamma p}^{0.32}$, and calculations according to the Ryskin model for gluon density functions are shown. Included are results from fixed target experiments[26].

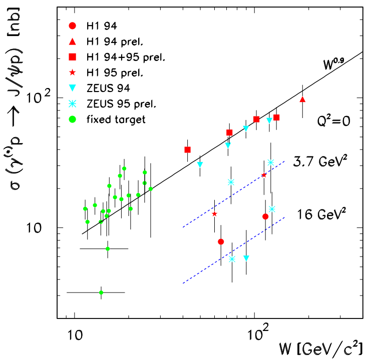

Figure 9: W-dependence of elastic J/Ψ production at high Q^2. Photoproduction results and measurements by fixed target experiments are also shown for comparisons.

A good description of the rise in the cross-section is given by calculations within the Ryskin model[27]. In figure 8, curves are shown for two parametrizations of the gluon density (MRSA' and GRV). The absolute normalization of the calculations is not reliable, so that only the shapes should be compared.

3.3 J/Ψ Production in DIS [28]

The elastic interaction $\gamma^* p \to J/\psi p$ has been studied at an average Q^2 of about 16 GeV^2 in events where in addition to the decay products of the J/Ψ , a scattered positron is found. Comparing the cross-sections as measured by the H1 and ZEUS experiments (fig. 9), with those from fixed target experiments, a rise with $W_{\gamma p}$ similar to that seen in photoproduction events is observed. The measurements are compatible with a Q^2 evolution of the cross-section according to $1/(Q^2 + m^2_{J/\psi})^n$ with $n = 1.9 \pm 0.3$ (stat.).

3.4 Ψ' Photoproduction

Clear signals for $\psi(2S)$ are seen by searching for the decay to $J/\psi\pi^+\pi^-$ in the H1 detector where the J/Ψ subsequently decays to a lepton pair, and insisting that no further charged particles are identified. The acceptance is limited to the kinematic region $z > 0.95$, where a ratio for the photoproduction cross-sections, $\sigma(\psi')/\sigma(J/\psi) = 0.16 \pm 0.06$ at $W_{\gamma p} = 80$ GeV is measured. This ratio appears energy independent when comparing to measurements from other experiments [29] at $W_{\gamma p} < 20$ GeV.

4 Summary and Conclusions

The production of charm quarks in e^+p-collisions at HERA has been studied by identifying charm in the form of D, J/Ψ and $\psi(2S)$ mesons. All photoproduction cross-sections are found to rise steeply with increasing $W_{\gamma p}$. This characteristic is well described by calculations based on perturbative QCD in which the rise reflects the increase in the gluon content of the proton towards low x. The shape of differential distributions is in general rather well predicted within pQCD calculations, both in photoproduction and DIS. The charm contribution to F_2 is found to be large. No indications of colour-octett contributions are seen in inelastic vector meson production. QCD-based approaches are quite successful in describing diffractive J/Ψ production.

Acknowledgments

It is my pleasure to thank the organisers of the symposium for a very stimulating and intensive time in a magnificent surroundings. It's a pity we didn't get those late-comers of whales onto a T-shirt! I thank all H1 and ZEUS members who provided figures.

References

1. H1 Coll., I.Abt et al., DESY 96-001 (1996).
2. ZEUS Coll., J.Breitweg et al., DESY 95-193 (1995).
3. J.Binnewies, B.A.Kniehl and G.Kramer, DESY-97-012, 1997; B.A.Kniehl, G.Kramer and M.Spira, DESY-96-210, 1996.
4. M.Cacciari et al., Phys. Rev.D55, 2734 (1997); Z.Phys. C69, 459 (1995).
5. M.Cacciari and M.Greco, Phys. Rev. D55, 7134, (1997).
6. B.W. Harris and J. Smith, FSU-HEP-970527, 1997.
7. E. Laenen et al., Nucl.Phys. B392, (1993), 162 and 229.
8. M.A.G.Aivazis et al., SMU-HEP-92-04; Phys.Rev. D50, 3102, (1994).
9. H1 Coll., S Aid et al., Nucl. Phys **B**472 (1996) 32.
10. ZEUS Coll. J. Breitweg et al., Phys. Lett. B401, 192 (1997); Phys. Lett. B349, 225 (1995).
11. C.Peterson et al., Phys. Rev. D27, 105 (1983).
12. OPAL Coll., CERN-PPE-94/217 (1994); LEP Coll., CERN-PPE-96/017 (1996).
13. C.F.Weizsäcker, Z.Phys. 88, 612 (1934); E.J.Williams, Phys. Rev. 45, 729 (1934).
14. S.Frixione et al., Phys. Lett. B348, 633 (1995); Nucl. Phys. B454, 3 (1995).
15. H1 Coll., C.Adloff et al., Z.Phys. C72, 593 (1996).
16. ZEUS Coll. J.Breitweg et al., DESY-97-089.
17. H1 Coll., S.Aid et al., Nucl. Phys. B472, 3 (1996).
18. ZEUS Coll. J.Breitweg et al., DESY-97-147.
19. M.Krämer et al., Phys. Lett. B348, 657 (1995).
20. M.Krämer, Nucl. Phys. B459, 3 (1996).
21. CDF Coll., Phys. Rev. Lett. 69, 3704 (1992).
22. ZEUS Coll. J.Breitweg et al., Z.Phys. C75, 215 (1997).
23. A.Donnachie,P.V.Landshoff, Phys. Lett. B348, 213 (1995); B296, 227 (1992).
24. M.Cacciari,M.Krämer, DESY 96-005 (1995).
25. M.G.Ryskin, Z.Phys. C57, 89 (1993).
26. E687 Coll., Phys. Lett. B316, 197 (1993); E401 Coll., Phys. Rev. Lett. 48, 73 (1982); FTPS Coll., Phys. Rev. Lett. 52, 795 (1984)
27. M.G.Ryskin et al., DTP-95-96 (1995), revised Feb 1996.
28. H1 Coll., S.Aid et al., Nucl. Phys. B468, 3 (1996).
29. EMC Coll., Nucl. Phys. B213, 1 (1983); NA-14 Coll., Z.Phys. C33, 505 (1987); E401 Coll., Phys. Rev. Lett. 50, 302 (1983)